Acta Materialia 292 (2025) 121041

Contents lists available at ScienceDirect

Acta Materialia

journal homepage: www.elsevier.com/locate/actamat

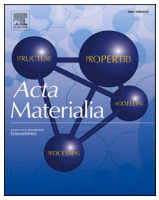

Full length article

Grain boundary properties and microstructure evolution in an Al-Cu alloy

Zipeng Xu [a], Jun Sun [b], Jules M. Dake [c], Jette Oddershede [b], Harpreet Kaur [d], S. Kiana Naghibzadeh [d], Carl E. Krill III [3], Kaushik Dayal [d], Gregory S. Rohrer [a,1,*]

[a] Department of Materials Science and Engineering, Carnegie Mellon University
[b] Xnovo Technology ApS, Galoche Allé 15, 1st floor, 4600 Køge, Denmark
[c] Institute of Functional Nanosystems, Ulm University, 89081 Ulm, Germany
[d] Department of Civil and Environmental Engineering, Carnegie Mellon University

ARTICLE INFO

Keywords:
Grain boundary
Grain growth
3D microstructure
Xray Microscopy

ABSTRACT

Grain boundary (GB) properties in an Al-5 wt % Cu alloy have been extracted from diffraction contrast tomography images after 10 sequential annealing steps for 15 min at 630°C. At the annealing temperature, a copper-rich liquid was present at the GBs. The growth and shrinkage of the grains are strongly correlated with the grain size, and the velocity of individual boundaries is strongly correlated with boundary mean curvature, as expected from the classical theory of coarsening. The experimental results compare well to a threshold dynamics grain growth simulation of the process assuming uniform grain boundary energies. The correlation of the interface velocity and curvature is observed both for the data on average and for certain commonly occurring grain boundary disorientations. It is also found that the curvatures and relative areas of GBs depend on the five grain boundary parameters, even though the GBs are formed in conditions of low energy anisotropy. The observations are compared to results from grain growth in the solid state, where strong correlations between interface velocity and curvature are not observed.

1. Introduction

When polycrystalline microstructures are heated to sufficiently high temperatures, the average crystallite size increases. There are two limiting conditions for this process. If the material is a single-phase solid, the grain size increases through the migration of grain boundaries, and we refer to this process as grain growth. On the other hand, if crystals of a single phase are separated by an intervening phase (solid or liquid), then the increase in crystal size occurs by the diffusion of material from one crystal to another through the intervening phase; we refer to this process as coarsening. The conventional mean field theories for grain growth [1] and coarsening [2–4] are quite similar in the sense of assuming that growth rates depend on a crystal's relative size in comparison to the mean size. Both theories predict that grains smaller than the mean should shrink and disappear with time, while larger grains should increase in size. The mechanism is assumed to be the curvature of the crystal boundaries– or more typically some inverse measure of the crystal size. Smaller crystals have a greater curvature relative to the mean and therefore lie at a higher chemical potential, whereas larger crystals have a lower chemical potential. The result is that material is transferred from the smaller to larger crystals. For the case of grain growth, the concept is generalized to the condition that grain boundaries migrate towards their centers of curvature at a rate proportional to the curvature [5,6].

The recent development of X-ray microscopy [7,8] has made it possible to follow the evolution of the shapes and sizes of crystals within a polycrystal during annealing, making it feasible to test the accepted theories for grain growth and coarsening. The findings for grain growth have been surprising. For example, observations indicate that a grain's relative size [9,10] and mean width [11] are poor predictors of whether or not the grain will shrink or grow. Several other measurements [12–14] and simulations [15–17] indicate that the sign of a grain boundary's curvature is a poor predictor of the direction the grain boundary will migrate and that it is not possible to assign consistent mobilities to grain boundaries based on their curvature and velocity [18]. The findings contradict experimental observations of the

* Corresponding author.
E-mail address: rohrer@cmu.edu (G.S. Rohrer).
[1] Gregory S. Rohrer was an Editor of the journal during the review period of the article. To avoid a conflict of interest, Gregory S. Rohrer was blinded to the record and another editor processed this manuscript

https://doi.org/10.1016/j.actamat.2025.121041
Received 18 November 2024; Received in revised form 7 March 2025; Accepted 11 April 2025
Available online 12 April 2025

migration of isolated boundaries in idealized bicrystals [19] and the classical model for grain boundary migration [6]. The analysis of past 3D coarsening experiments has focused on grain rotation rather than growth rates, but these studies have observed increased growth rates for larger crystals [20,21].

Grain boundary energy anisotropy has been suggested as one of the possible reasons that grain boundary migration in polycrystals is not predicted by curvature alone [22]. If this were true, then we can hypothesize that in the absence of grain boundary energy anisotropy, curvature should predict the direction and velocity of migration. While grain boundaries with isotropic energies do not exist (except, perhaps, very near the melting point), this condition is approximated by coarsening processes during which the microstructure evolves in the presence of a liquid phase between the grains. Therefore, the only energy anisotropy is that of the solid-liquid interface, which is expected to be weak compared to the grain boundary energy anisotropy. The presence of a liquid phase also guarantees that no grain boundary dislocations or disconnections are involved in the migration process, that interface migration is not driven by stress, and that there are no triple lines to influence interface dynamics.

An ideal material for this experiment is an Al-5 wt % Cu alloy, used in previous coarsening experiments [20,21]. When heated to 630°C, 30 vol % of the sample is a Cu-rich liquid and 70 vol % remains solid Al saturated with Cu [23] (see Fig. S1). Previous work has shown that the liquid wets the grain boundary regions, so at the annealing temperature, the sample is made of solid Al grains surrounded by a Cu-rich liquid [20]. When the sample is cooled below the solidus at 560°C, the liquid in the intergranular regions solidifies, and grain boundaries re-form between grains of the aluminum-rich solid solution phase (details of the microstructure are described in the supplemental information). Data from this material, acquired after ten sequential anneals for 15 min at 630°C, has been made available as the result of previous research [21,24]. In the current work, the properties of the grain boundaries are analyzed in the solid state at room temperature, recognizing that their changes in position occurred by coarsening rather than grain boundary migration. The presence of a liquid phase during annealing also means that there will be significant changes in the microstructure during sample solidification. Nevertheless, we assume that the volumes of grains after solidification are representative of those at high temperature and that the curvatures, which depend most on grain size, are also representative.

The purpose of this paper is to compare interface curvatures to interface velocities and test the hypothesis that the migration of interfaces during coarsening is driven by capillary forces and is therefore correlated with the curvature. It is shown that the evolution of the microstructure compares well with the classical theory, unlike phenomena observed during grain growth in the solid state. Surprisingly, the distribution of grain boundary planes that form after solidification is similar to that found in Al annealed in the solid state, [25] suggesting that the anisotropy of the energy of the grain boundary plane influences the grain boundary plane orientation after solidification.

2. Experiments and Simulations

2.1. Materials and measurements

A detailed description of the Al-5 wt % Cu sample preparation and data collection methods can be found in the report by Dake et al. [20], which focused on analyzing grain rotations during annealing [21]. The information needed to understand the present analysis is related in the remainder of this paragraph. The sample has the FCC crystal structure and a cylindrical shape (1.4 mm in diameter and 6.5 mm in height). After an initial 20 min anneal, the microstructure experienced ten sequential 15 min heat treatments at 630°C, each followed by an air-quench. At room temperature after each anneal, a high-resolution (1.84 μm) absorption contrast tomograph (ACT) image was formed to visualize the copper-rich interface, and a three-dimensional orientation map was measured using lab-based diffraction contrast tomography (DCT).

The measured orientation maps were reconstructed using GrainMapper3D [26]. The entire material was reconstructed as FCC-structured Al; any phase separation that likely occurred when the liquid solidified was not resolved in the DCT images. The microstructure was reconstructed on a grid of cube-shaped voxels with dimensions $6 \times 6 \times 6$ μm^3. Grains were segmented using a 1° disorientation threshold. The data was then further analyzed using the open source software Dream.3D [27]. The resulting initial (denoted as t0) and final (denoted as t10) reconstructed microstructures have 1934 and 934 grains, respectively, and the average grain radius increased from 107 μm to 136 μm. All grains intersecting the top and bottom of the field of view were excluded from the analysis.

2.2. Interface curvature calculation

The original stair-stepped voxelated interfaces after reconstruction must be smoothed to obtain reasonable grain boundary property distributions. Two Dream.3D [27] filters, "Quick Surface Mesh" and "Laplacian Smoothing," were applied to the voxelated structure. The former filter replaced the stair-stepped interfaces with triangular meshes, and the meshes were then further smoothed by the "Laplacian Smoothing" filter, using 100 iterations and a weighting factor of 0.025. After meshing and smoothing, each grain boundary is described by a set of contiguous triangles. The triangles share the same two grain orientations on either side, but have distinct normal vectors in the crystal frame as well as areas. We can assign other grain boundary properties to each triangle. For example, the grain boundary local curvature is determined by the Cubic-Order algorithm [28] implemented in Dream.3D. As a result, two principal curvatures (κ_1, κ_2) and related principal directions for each meshed triangle were determined, and the corresponding mean curvature for that triangular interface was calculated as $(\kappa_1+\kappa_2)/2$. The individual triangle mean curvatures separating two grains can be averaged to determine the mean curvature of the entire grain boundary, and all triangles surrounding a single grain can be averaged to determine the normalized integral mean curvature of a grain. The quantities are calculated using a previously described method [29].

As noted in the introduction, the curvatures were measured in the room-temperature state, and the grain shapes differ from those at the annealing temperature. Based on images of two-phase microstructures, [30,31] we expect the grains at high temperature to take on compact concave shapes, with their formerly solid outer surfaces now in the liquid state, as dictated by the conditions of two-phase equilibrium. The main difference is that the liquid phase eliminates triple lines, replacing them with smoothly curved surfaces. The individual grain faces are assumed to maintain approximately the same dimensions, but be proportionally smaller. The curvature of one of the faces will change sign, but our grain boundary curvature measurement is unsigned. Therefore, while the high-temperature and room-temperature curvatures are not identical, we still expect the room-temperature curvature to be strongly correlated with the unknown high-temperature curvature.

2.3. Interface relative energy calculation

Grain boundary relative energies can be calculated from the geometry of the triple lines [32]. To determine the triple line geometries, the initial 3D structure was interpreted as a series of parallel two-dimensional orientation maps. Within each layer, the grain boundaries were represented as a series of line segments. Triple points on each layer were identified as the location where three different grain boundary segments meet. The orientations of grains around triple points on adjacent layers were compared to identify points belonging to the same triple line; the triple lines were then defined by connecting these points on adjacent layers. Knowing the in-plane grain boundary

segments and the triple lines, the grain boundary normal and area can be calculated. To determine the grain boundary energies, it was assumed that the junction geometries satisfy the Herring condition, [33] and the locally optimal block preconditioned conjugate gradient method (LOBPCG) [34] was used to solve the system of equations defined by the Herring condition to find the capillarity vectors and minimize the differences between the boundaries and their neighbors in crystallographic space, as previously described in detail [32]. The relative energy of each boundary can then be determined by the product of its plane normal and the corresponding capillarity vector.

2.4. Interface migration velocity calculation

The first step in determining grain boundary velocity is to track the grains from one annealing step to the next, so that we can identify the same grain boundary in two annealing states. If two grains in adjacent time steps were misoriented by less than 10° and their centroids were separated by less than 200 μm, they were assumed to be the same grain. Using these criteria, on average, 99.88 % of the grains in the latter of two time steps could be matched to grains in the previous time step. The second step in the analysis procedure is to ensure that the orientation maps at each time step are spatially aligned. Following the method described previously, [12] we calculated the average disorientation between all of the voxels in one map and the map in an adjacent time step for relative translations $i\vec{x}$, $j\vec{y}$, $k\vec{z}$, for all combinations of indices i, j, and k from -4 to +4, where $\vec{x}$, $\vec{y}$ and $\vec{z}$ have lengths equal to the voxel side length. The translation vector with the minimum average disorientation was assumed to be the best alignment.

Once the grains were identified and aligned, we employed a method described previously [12] to calculate the boundary velocity. Briefly, the velocity of the boundary between grains m and n can be determined by counting the volume of voxels that changed their grain IDs from m to n from one annealing state to the next and dividing by the product of annealing time (Δt) and average grain boundary area ($\overline{A}_{mn}$). The average boundary area was calculated by averaging the measured areas of the (same) grain boundary at the two time steps.

2.5. Grain boundary properties distribution analysis

Using the analysis described above, we can specify the disorientation, plane normal direction, area, energy, curvature, and velocity of each triangular mesh element or each grain boundary as a whole. Therefore, we know the distribution of these properties as a function of all five crystallographic grain boundary parameters. To plot grain boundary plane distributions at fixed disorientation or in the crystal reference frame, we used the method of Glowinski and Morawiec, [35] as implemented in 3D_dist_graph [36]. Specific points in each distribution (fixed disorientation and grain boundary plane orientation) were sampled from the data using a 5° tolerance for disorientation and 7° tolerance for the plane normal.

2.6. Grain growth simulation

The threshold dynamics (TD) technique was used to simulate grain growth using the observed Al-Cu microstructure as a starting point. This method simulates the migration of grain boundaries through mean curvature [37,38]. Although the microstructure in the experiment is evolving by coarsening, we employ a grain growth model because the objective is to compare the experimental outcome to isotropic grain growth. Here, we implemented the method as described in detail in a previous publication [39] using an available code [40] but also provide a brief summary here. In the TD method, each grain has a characteristic function with value one within the grain and zero outside the grain. To simulate the evolution of the observed microstructure, each grain's characteristic function is convolved with a Gaussian kernel. In this step, the kernel is positioned with its maximum at each grid point in the simulation and the convolution operator computes the integral of the product between the characteristic function and the kernel. When the boundaries of the kernel fall completely outside or within a grain, the convolution yields the trivial values of zero or one. However, when there is some overlap between the non-zero part of the kernel and the non-zero part of the characteristic function, the convolution value depends on the shape of the grain, which carries information about the curvature. After the convolution values have been assigned to each point, a threshold is applied so that values greater than 0.5 are assigned to one and less than the threshold value are assigned to zero, effectively moving the boundaries. Using the same kernel for each boundary is equivalent to the assumption that all grain boundaries have the same energy, and using a Gaussian kernel is equivalent to assuming the energy is the same in all directions.

It was necessary to crop the data in the vertical direction from 1133 to 226 layers to stay within computational hardware limitations and memory requirements. This cropping was guided by the set of alignment vectors introduced in Section 2.4, ensuring that the same grain regions were consistently selected across all annealing time steps of the experimental data.

The initial average grain size was calculated from the grains that did not intersect any of the boundaries of the sample volume. The simulation was evolved with a time step size of 10^{-5} (in the TD method, the time step is related to the variance of the Gaussian kernel) [39] until the grain size in the simulated volume matched as nearly as possible the measured average grain size in the Al-Cu sample at the next annealing step. The procedures for the analysis of the simulated volume were identical to those used for the experiment.

3. Results

A typical cross section of the material is illustrated in Fig. 1. In the ACT image (Fig. 1a), the lightest contrast areas correspond to Cu-rich regions, the darker gray regions are Al, and the darkest regions are voids, presumably formed by drainage of the Cu-rich liquid when molten [21]. An inverse pole figure (IPF) map (Fig. 1(b)) derived from the DCT data taken at approximately the same position shows the Al orientations in a similar area. Even though the ACT image has a higher resolution than the IPF map, and the Cu-rich regions were assumed to be identical to the Al, the grain shapes in the two images are comparable, as reported previously [41].

The initial microstructure contained 1934 grains with an average equivalent-sphere radius of 107 μm. As a result of the sequential heat treatments, the final microstructure contained 934 grains with an average radius of 136 μm. The coarsening of the microstructure was reflected by a decrease in the total grain boundary area per volume, as illustrated in Fig. 2. Voorhees and co-workers have refined the theory for the coarsening of a high-volume fraction of solid with non-spherical shapes [2,3,30,42,43]. One feature that emerged from these studies was that the inverse of the surface-to-volume ratio increased linearly with the cube root of time, [43] which Fig. 2 illustrates is also a characteristic of our data. Although the grain boundary area per volume changed during the experiment, other normalized quantities, such as the grain boundary disorientation distribution, remained essentially constant throughout the experiment (see Fig. S2). Therefore, the measurements at each time step were combined to evaluate the distributions of microstructural metrics.

In coarsening, it is normally assumed that the smallest grains will shrink with time and the largest grains will grow. The grain volume change data in Fig. 3, which aggregates data from all of the time steps, is consistent with this expectation. Grains with radii smaller than 120 μm (fewer than 12 neighbors at room temperature) mostly shrink with time, and grains with larger sizes and more neighbors mostly grow with time. Note that the growth rate crosses zero very near the mean grain size and the mean number of neighbors. We note that there is a distribution of

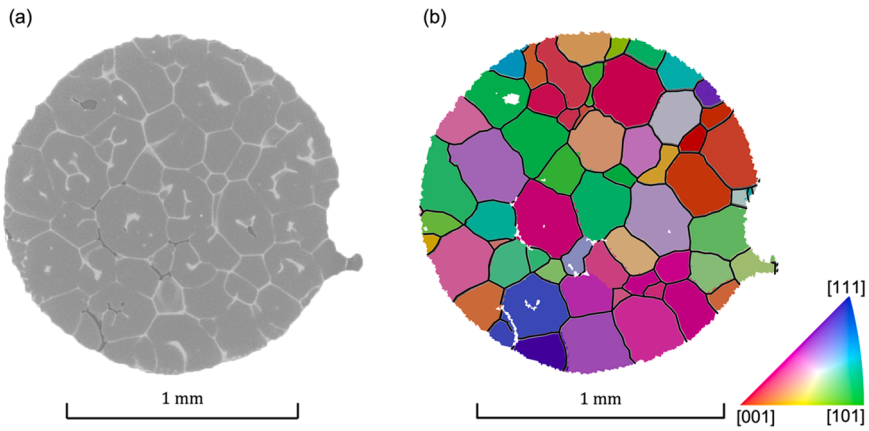

Fig. 1. An example of a cross-section of the Al-Cu alloy at t_0 measured by (a) ACT and (b) DCT. The black lines in (b) mark the locations of grain boundaries, and the white regions are unindexed void space.

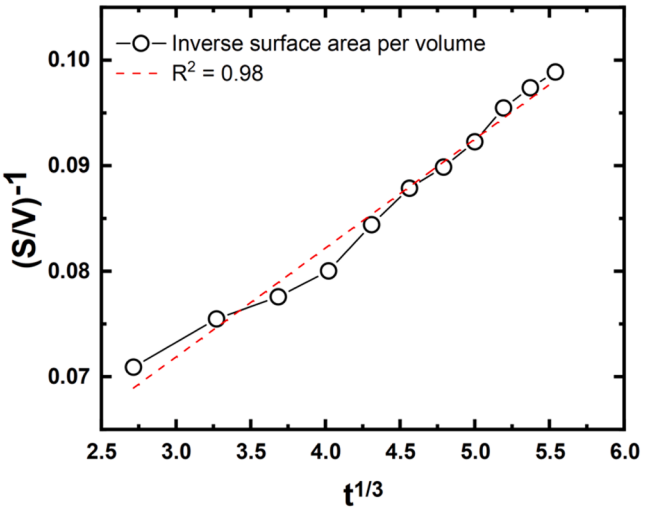

Fig. 2. The inverse of the surface-to-volume ratio versus the cube root of time for the Al-Cu alloy. The dashed line shows a linear fit.

observations that are used to determine the mean at each grain size, and the standard deviation of this distribution shows that some of the individual observations have signs that differ from expectation. The apparent decrease in shrinkage rate at small grain sizes reflects the fewer number of voxels present in these small grains. It is noteworthy that when the same statistic was evaluated for solid-state grain growth in Ni [9] and Fe, [10] the findings did not show this behavior, even though the same analysis methods were used.

Under the assumption that interfaces in the alloy are driven by capillary forces, the volumetric grain growth rate (dV/dt) is [44]

$$\frac{dV}{dt} = V^{\frac{1}{3}} M \gamma \wp', \tag{1}$$

where V is the initial grain volume, M is the interface mobility, γ is the interface energy, and $\wp'$ is the normalized integral mean curvature of the grain. If the interface mobility and energy are assumed to be constant, then dV/dt should be directly proportional to $V^{\frac{1}{3}}\wp'$, which is demonstrated in Fig. 4. Eq. 1 predicts the correct growth direction for 76 % of the 11720 grains, the mean growth rates vary linearly with $V^{\frac{1}{3}}\wp'$, and the growth rate at $V^{\frac{1}{3}}\wp' = 0$ is also zero; these observations indicate that Eq. 1 provides a reasonable description of the microstructural evolution of this alloy. It should be noted that the curvatures are measured from the DCT data, so the grain shapes are not identical to the shapes existing at elevated temperature when the liquid was present.

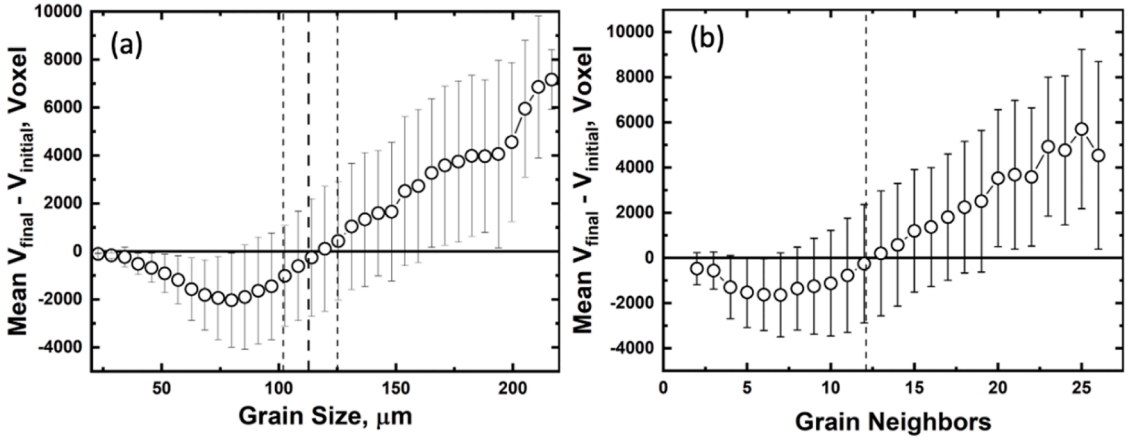

Fig. 3. Change in the grain volume (V) versus (a) grain size and (b) number of grain neighbors. The circles show the mean volume for each category on the horizontal axis and the bars show one standard deviation for the distribution of the data within that category. From left to right, the three dashed lines in (a) mark the initial mean size of matched grains, the mean size of all matched grains in the experiment, and the final mean size of matched grains. The dashed line in (b) marks the mean number of grain sides.

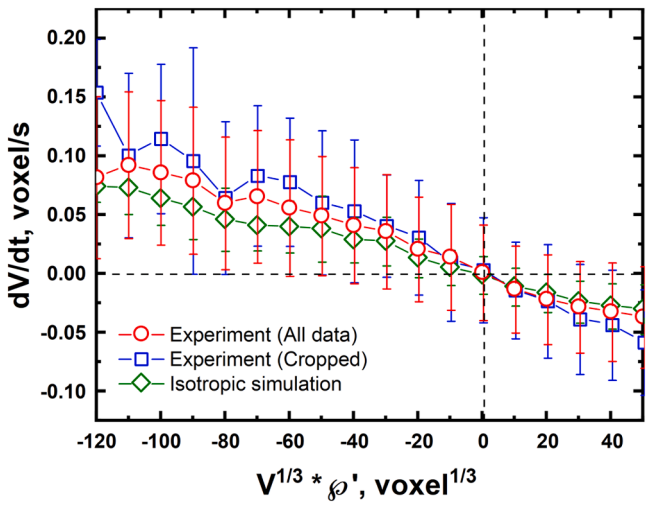

Fig. 4. The correlation between the grain volume rate of change dV /dt and the product $V^{\frac{1}{3}}\wp'$ for all experimental data (red circles), cropped experimental data (blue squares) and isotropic simulation data (green diamonds). Each marker indicates the mean, and the bar represents the width of the distribution (± one standard deviation).

The results for the subset of experimental data used for the simulation ("cropped" data) and the simulation results are also shown in Fig. 4. These data have about $1/6^{th}$ the number of grains as the complete experimental data. These results are similar to the complete experimental data in that they approximate a line that passes through the origin. For these subsets, the sign of the growth rate is correctly predicted for 78% (cropped) and 87% (simulation) of the grains. The consistency of the simulation and the experiment indicates that isotropic grain growth and the coarsening of a high-volume fraction solid depend on curvature in the same way, even if the atomic scale mechanisms differ.

While the volumetric growth rate considers changes that occur to the overall grain, we can also measure the velocities of the individual boundaries. It should be noted that we again use the boundary shapes determined at room temperature, following migration of the interface separated by liquid. The correlation between the mean velocity and the boundary curvature is presented in Fig. 5(a). Note that the curvatures are the mean curvature of the entire grain boundary and that each point is the mean of a broad distribution with an average standard deviation of 7.5×10^{-8} mm/s. There is a strong correlation between grain boundary velocity and curvature for the curvature range from 0 to 3.25 mm^{-1} (containing 94.5 % of 64670 grain boundaries). For curvatures greater than this range, the slope of the data changes. It should be noted that there are fewer boundaries in this range, so the mean of the velocity distribution is likely to have more uncertainty. The results for the subset of the data that was simulated are shown in Fig. 5(b) (containing 94.1 % of 14054 grain boundaries). Both show a linear relation between velocity and curvature, but the velocities of the boundaries in the simulation are less than those in the experiment. The mean velocities are lower in the simulation because it eliminates more small grains than the experiment [39], selectively excluding some fast moving boundaries from the distribution.

The grain boundary disorientation distribution with 1° resolution of the Al-Cu alloy is compared to the random distribution in Fig. 6. The results show that the disorientation distribution is nearly random except for two features that are observed with population greater than twice the random expectation: there are more low-angle grain boundaries (LAGBs) than expected and more grain boundaries at 60°. The high population of LAGBs has been observed in other textured materials [45, 46] (the sample has a cube texture with an intensity of approximately 3 multiples of random distribution (MRD)), and the local maximum at 60° probably results from Σ3 (60°/[111]) grain boundaries that are common in FCC structured materials.

The grain boundary area distributions at fixed disorientation showed more significant anisotropy than the disorientation distribution alone, with some grain boundary planes occurring with populations more than 20 times the random value. Note that these area distributions reflect the state of the solidified microstructure, rather than the microstructure during coarsening; we find it surprising that they display anisotropic distributions, unlikely to be associated with the more isotropic solid-liquid interface energy distribution at the maximum temperature. The grain boundary area, curvature, velocity, and energy distributions are illustrated in Fig. 7 for the Σ3 grain boundaries (a-d) and LAGBs (e-h), two of the most frequently observed boundaries. For the Σ3 grain boundaries, the maximum area is located at the twist orientation, and the minimum is at the $\{\bar{1}01\}$ tilt boundaries. For the LAGBs, the opposite occurs, with the maximum area found at the position of the $\{\bar{1}\bar{2}\ 11\ 1\}$ symmetric tilt grain boundaries, and the minimum at the position of the twist grain boundary. For both grain boundary classes, there is an approximate inverse correlation between the relative area and the grain boundary relative energy, although the variations in energy are relatively small. Finally, the velocities of both GB classes show an approximate correlation with the mean grain boundary curvature, as also evident in Fig. 5. Note, however, that the mean curvatures in Fig. 7 are for individual triangles, while those in Fig. 5 are averaged over entire boundaries. When all of the points in Fig. 7(c) are plotted against the points in Fig. 7(b), the data fit a line with $R^2 = 0.94$ (see Fig. 8).

As noted previously, the data in Figs. 3 through 8 were consolidated from all of the time steps in the experiment. Other than the increase in mean grain size and the decrease in mean curvature, the only other significant change noted was an increase in the relative areas of coherent twin boundaries, which rose from approximately 18 MRD to 32 MRD (see Fig. 9). Note that the total number of Σ3 grain boundaries decreased from 214 to 81 during annealing. Therefore, the increase in area fraction of coherent Σ3 boundaries does not mean that their areas necessarily increased, but that they make up a larger fraction of the total boundary area. This indicates that Σ3 boundaries are less likely to be eliminated in comparison to other boundaries during coarsening.

4. Discussion

The influence of curvature on the growth of crystals in a solid-liquid mixture has been established by earlier studies [47]. From this perspective, the results reported in Figs. 2 through 5 are consistent with expectations. These correlations provide strong evidence that the coarsening of the Al grains in this alloy is predicted by curvature. It should be emphasized that a distribution of observations contributes to each mean value (for example, note the bars in Figures 3 and 4), and some of the points do not follow the expected trends. Several factors might contribute to this scatter. First, the curvature measured in the solid state is only an approximation of the true curvature present in the two-phase material at elevated temperature. Second, the curvature measurement is based on meshing of the interface, and this is an approximation of the true interface. Beyond these experimental limitations, there are also local variations in curvature at places where multiple grains approach each other that are not captured by the assignment of a single mean curvature to each boundary. Despite these limitations associated with the method, the trends illustrated in the mean values are consistent with the classical theory of coarsening.

A unique feature of the present work is that we were able to track individual interfaces by their crystallographic character. As a result, we were able to examine the correlation between curvature and velocity for specific types of boundaries. The results in Fig. 8 show that the correlation is very strong for the Σ3 boundaries, which are the most frequently observed grain boundaries. We note that there is a trend that the highest population grain boundaries (lowest energy) have the

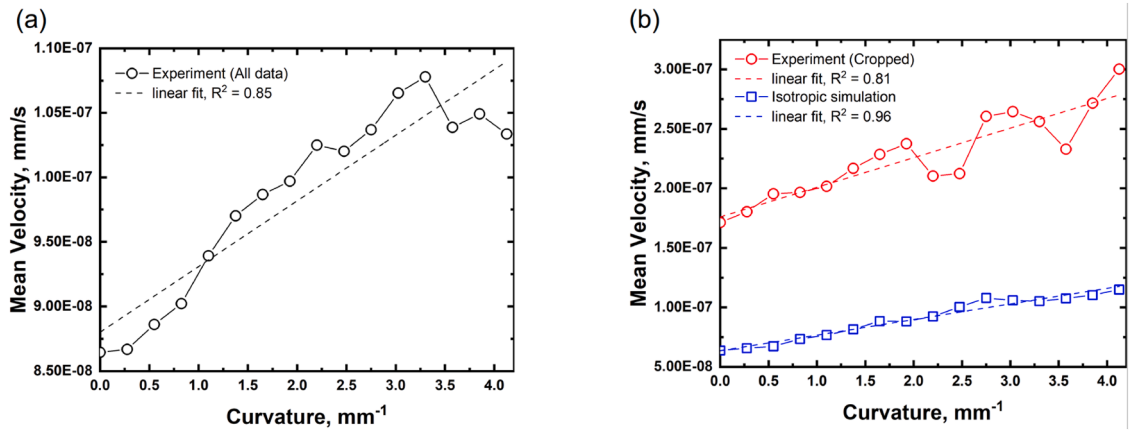

Fig. 5. The grain boundary velocity plotted against GB curvature for the microstructures. (a) All experimental data, with a bin width of 0.275 mm^{-1} and linear fit $R^2 = 0.85$; the average standard deviation at each point is 7.5×10^{-8} mm/s. (b) Comparison between the simulated subset of experimental data (red circles) and the corresponding simulation result (blue squares). The bin width is 0.275 mm^{-1}, the linear fit R^2 values are 0.81 and 0.96, and the average standard deviations at each point are 3.6×10^{-7} mm/s and 6.3×10^{-8} mm/s for the experimental subset and the simulation, respectively.

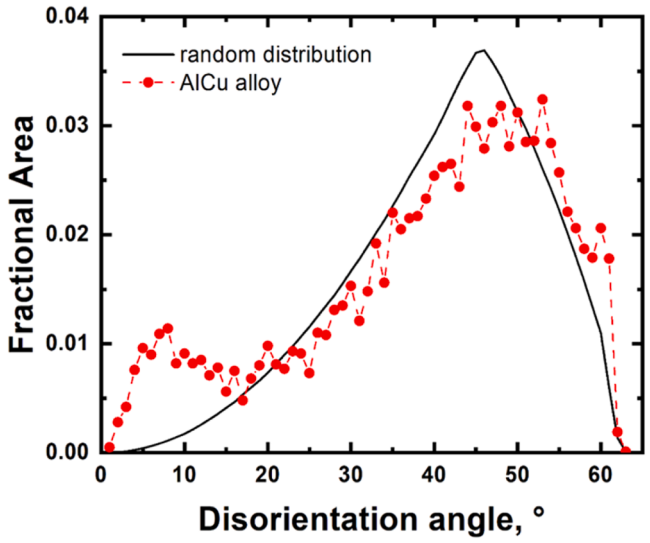

Fig. 6. The disorientation distribution with 1° resolution for the Al-Cu alloy, with data from all time steps aggregated (red), compared to the random disorientation distribution (solid black curve).

smallest velocities and curvatures, while the grain boundaries with the largest velocities and curvatures have smaller relative areas. This suggests that boundary kinetics might hamper our ability to observe the highest velocity boundaries. A similar trend is observed for the LAGBs (Fig. S3a) and the Σ11 boundary (Fig. S3b). The velocities and curvatures of grain boundary types with relative areas less than 3 MRD do not manifest strong correlations, but it is unclear if this is because of an insufficient number of observations or because these boundaries are fully wet at the annealing temperature and, in that condition, their properties no longer depend on the orientation of the grain boundary plane. The fact that the scatter in the correlation in Figs. 8 and S3 increases for lower-population boundaries suggests that the number of observations may play a role.

Another interesting aspect of the findings is the anisotropy of the grain boundary plane distribution. For the LAGBs and Σ3 boundary distributions shown in Fig. 7, there is relatively strong anisotropy, with the preferred planes having areas more than four times greater than the non-preferred planes. The Σ11 {1 $\bar{1}$ 3} boundary, which has a disorientation of 50.5° around [110], (see Figs. S4 (a) and (b)) provides another example of a low-energy, high-population grain boundary. These distributions are similar to those reported for commercially pure Al [25]. Because the grain boundary plane anisotropy is inversely correlated with the grain boundary energy anisotropy during grain growth, [48] and the observed energy anisotropy is weak (as expected), the grain boundary plane distributions ought to exhibit weak anisotropy. There are two possible explanations for why this was not the case. The first is that the lowest-energy boundaries at the maxima of these distributions are not wet by the Cu-rich liquid and, therefore, behave more like the grain boundaries in Al that have been characterized in the past [25]. Evidence for the anisotropic wetting of grain boundaries in Al-Ga alloys is well documented [49,50]. The second is that after solidification of the boundary regions, the interfaces can change their orientations to maximize the fractional areas that occupy orientations with the energy minima. Based on the current data, acquired after the solidification and cooling are complete, it is not possible to discriminate between these two cases.

It is also noteworthy that the relative area of coherent twin boundaries increased as annealing proceeded. The same phenomenon has been observed in solid-state grain growth [9]. An increase in the relative area of low-energy grain boundaries with annealing time has been explained by the preferential annihilation of higher-energy (smaller-area) boundaries during grain growth, a process that leads to a distribution of GB energies inversely correlated to area [51]. With a liquid separating the two grains, such a mechanism does not seem possible. The increasing relative area of the coherent twin boundaries with annealing time in this coarsening experiment might instead be the result of their low migration velocity.

While this is a study of coarsening, the results inform our interpretation of earlier solid state grain growth studies. First, earlier failures to detect correlations between curvature and grain volume changes or curvature and grain boundary velocity were not the result of limitations intrinsic to the methods or analysis [12–14]. The same methods applied to this Al-Cu alloy extracted robust correlations. The main difference is that, in the earlier studies, the microstructures evolve in the solid state, whereas in the present study, most, if not all, of the grain boundaries were replaced by solid-liquid interfaces. This suggests that the factors that influence grain boundary migration in the solid state differ in a significant way from the migration of boundaries during coarsening. Considering the difference in the mechanism, this finding might not seem surprising; however, the classical theories for both processes [1,4] are based on curvature, and they lead to similar predictions for the correlation between grain size and grain volume changes. While these predictions are consistent with the results of this coarsening experiment,

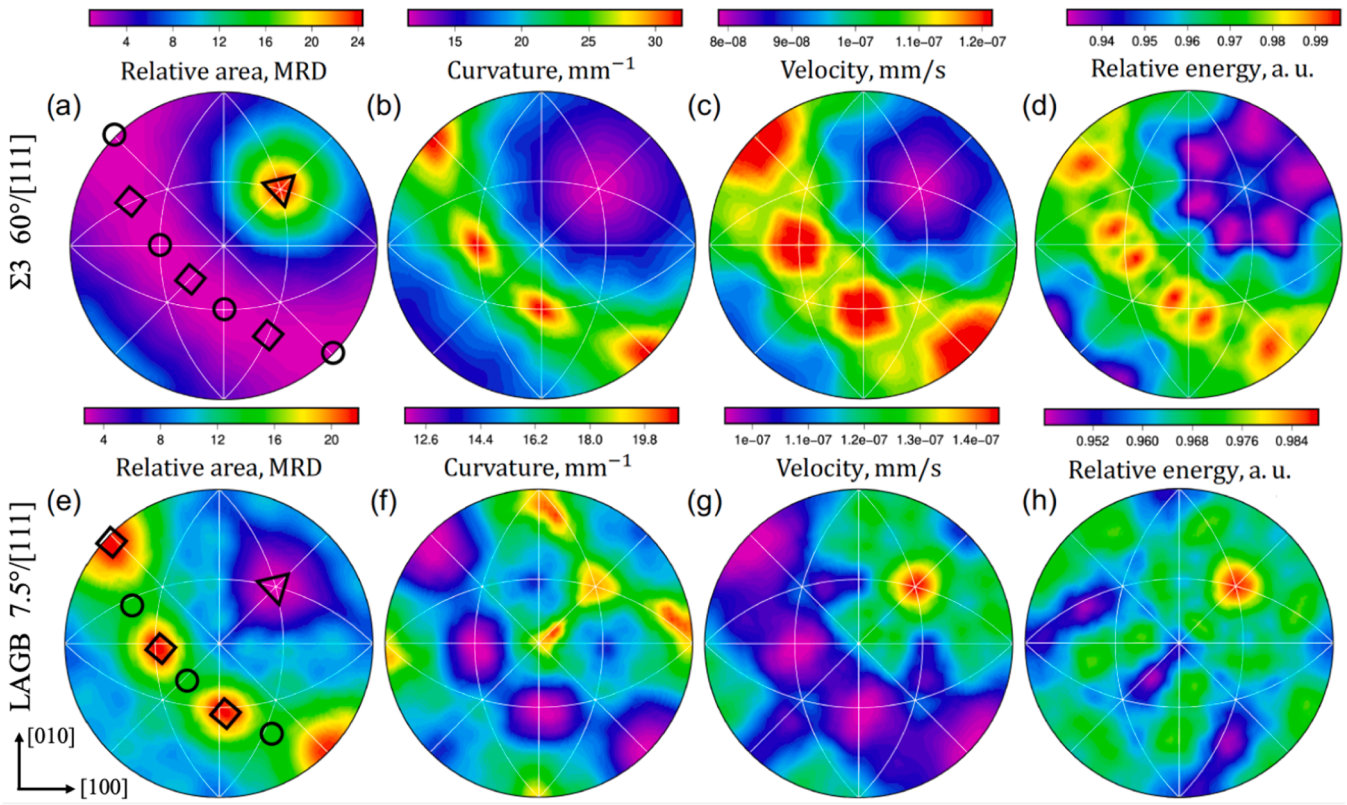

Fig. 7. Grain boundary relative area (a, e), curvature (b, f), velocity (c, g), and the relative energy (d, h) distributions plotted on stereographic projections along the [001] direction. Panels (a-d) are for boundaries with a 60°/[111] disorientation. There were 1147 distinct boundaries in this category comprised of 1.6 × 10^6 triangles. The orientations marked with a triangle, circles, and diamonds are the (111) twist boundary, {$\bar{1}$01} tilt boundaries, and {$\bar{2}$11} symmetric tilt boundaries, respectively. Panels (e-h) are for boundaries with a 7.5°/[111] disorientation. There were 833 distinct boundaries in this category comprised of 1.6 × 10^6 triangles. The orientations marked with a triangle, circles, and diamonds are the (111) twist boundary, {$\bar{7}$34} tilt boundaries, and {$\bar{1}\bar{2}$ 11 1} symmetric tilt boundaries, respectively.

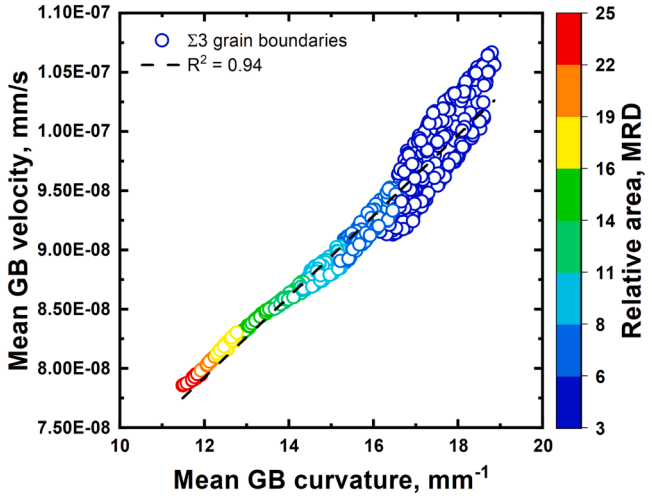

Fig. 8. The velocity and curvature of the Σ3 grain boundaries for the grain boundary plane normal with MRD > 3. A linear fit to the data shows a strong correlation. Each data point represents one grain boundary plane's normal orientation and is colored by the corresponding relative area, in MRD.

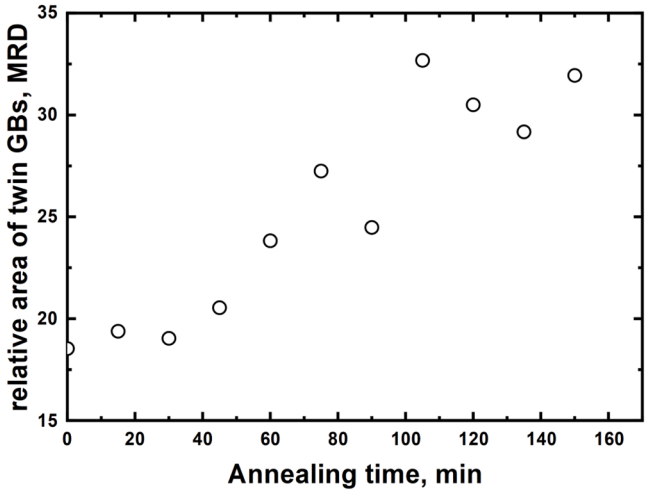

Fig. 9. The relative area of coherent twin boundaries plotted as a function of annealing time.

they contradict observations of solid state grain growth.

5. Conclusions

Grain boundary property distributions in an Al-5 wt% Cu alloy have been measured after 10 sequential 15 min anneals at 630°C. The results show that, although the microstructure evolved at a temperature at which the grain boundaries were replaced by a liquid phase, the resulting distribution of grain boundary properties shows clear anisotropy. In addition, at the grain level, the grain volume change can be correctly predicted by the grain size and the grain integral mean curvature, which is consistent with classical coarsening theory. At the level

of individual boundaries, the interface velocity shows a strong correlation with interface curvature, which was also found in isotropic solid-state grain growth simulations. The results indicate that, when the interface energy anisotropy is minimized and migration occurs by diffusion through the liquid, interface migration is correlated to curvature, contradicting what is observed during solid-state grain growth, where the grain boundary velocity and the curvature are not found to be strongly correlated.

CRediT authorship contribution statement

Zipeng Xu: Writing – original draft, Visualization, Validation, Methodology, Investigation, Formal analysis, Data curation, Conceptualization. **Jun Sun:** Writing – review & editing, Visualization, Validation, Software, Resources, Investigation, Formal analysis, Data curation. **Jules M. Dake:** Writing – review & editing, Visualization, Validation, Investigation, Formal analysis. **Jette Oddershede:** Writing – review & editing, Software, Resources, Investigation. **Harpreet Kaur:** Writing – review & editing, Visualization, Validation, Software, Data curation. **S. Kiana Naghibzadeh:** Writing – review & editing, Software, Investigation, Data curation. **Carl E. Krill:** Writing – review & editing, Supervision, Methodology, Data curation. **Kaushik Dayal:** Writing – review & editing, Supervision, Data curation. **Gregory S. Rohrer:** Writing – review & editing, Supervision, Resources, Project administration, Funding acquisition, Conceptualization.

Declaration of competing interest

The authors declare the following financial interests/personal relationships which may be considered as potential competing interests:

The author Gregory S. Rohrer is the Coordinating Editor for Acta Materialia and was not involved in the editorial review or the decision to publish this article.

Acknowledgments

This work was supported by the National Science Foundation under DMREF Grant No. 2118945.

Supplementary materials

Supplementary material associated with this article can be found, in the online version, at doi:10.1016/j.actamat.2025.121041.

References

[1] M. Hillert, On theory of normal and abnormal grain growth, Acta Metall 13 (1965) 227–238, https://doi.org/10.1016/0001-6160(65)90200-2.
[2] P.W. Voorhees, The theory of Ostwald Ripening, J. Stat. Phys. 38 (1985) 231–252, https://doi.org/10.1007/BF01017860.
[3] P.W. Voorhees, Ostwald Ripening of 2-phase mixtures, Ann. Rev. Mater. Sci. 22 (1992) 197–215, https://doi.org/10.1146/annurev.ms.22.080192.001213.
[4] C. Wagner. Theorie der Alterung von Niederschlägen durch Umlösen (Ostwald-Reifung), Zeitschrift für Elektrochemie, Berichte der Bunsengesellschaft für physikalische Chemie 65 (1961) 581-591, http://doi.org/10.1002/bbpc.19610650704.
[5] J.E. Burke, D. Turnbull, Recrystallization and Grain Growth, Prog. Metal Phys. 3 (1952) 220–292, https://doi.org/10.1016/0502-8205(52)90009-9.
[6] G. Gottstein, L.S. Shvindlerman, Grain Boundary Migration in Metals, CRC Press, Boca Raton, 2010.
[7] J.V. Bernier, R.M. Suter, A.D. Rollett, J.D. Almer, High-Energy X-Ray Diffraction Microscopy in Materials Science, Annu. Rev. Mater. Res. 50 (2020) 395–436, https://doi.org/10.1146/annurev-matsci-070616124125.
[8] W. Ludwig, S. Schmidt, E.M. Lauridsen, H.F. Poulsen, X-ray diffraction contrast tomography: a novel technique for three-dimensional grain mapping of polycrystals. I. Direct beam case, J Appl. Cryst. 41 (2008) 302–309, https://doi.org/10.1107/S0021889808001684.
[9] A. Bhattacharya, Y.F. Shen, C.M. Hefferan, S.F. Li, J. Lind, R.M. Suter, G.S. Rohrer, Three-dimensional observations of grain volume changes during annealing of polycrystalline Ni, Acta Mater 167 (2019) 40–50, https://doi.org/10.1016/j.actamat.2019.01.022.
[10] Y.F. Shen, S. Maddali, D. Menasche, A. Bhattacharya, G.S. Rohrer, R.M. Suter, Importance of outliers: A three-dimensional study of coarsening in alpha-phase iron, Phys. Rev. Mater. 3 (2019) 063611, https://doi.org/10.1103/PhysRevMaterials.3.063611.
[11] J. Zhang, Y.B. Zhang, W. Ludwig, D. Rowenhorst, P.W. Voorhees, H.F. Poulsen, Three-dimensional grain growth in pure iron. Part I. statistics on the grain level, Acta Mater 156 (2018) 76–85, https://doi.org/10.1016/j.actamat.2018.06.021.
[12] A. Bhattacharya, Y.F. Shen, C.M. Hefferan, S.F. Li, J. Lind, R.M. Suter, C.E. Krill, G. S. Rohrer, Grain boundary velocity and curvature are not correlated in Ni polycrystals, Science 374 (2021) 189–193, https://doi.org/10.1126/science.abj3210.
[13] V. Muralikrishnan, H. Liu, L. Yang, B. Conry, C.J. Marvel, M.P. Harmer, G. S. Rohrer, M.R. Tonks, R.M. Suter, C.E. Krill III, A.R. Krause, Observations of Unexpected Grain Boundary Migration in $SrTiO_3$, Scripta Mater. 222 (2023) 115055, https://doi.org/10.1016/j.scriptamat.2022.115055.
[14] Z.P. Xu, Y.F. Shen, S.K. Naghibzadeh, X.Y. Peng, V. Muralikrishnan, S. Maddali, D. Menasche, A.R. Krause, K. Dayal, R.M. Suter, G.S. Rohrer, Grain boundary migration in polycrystalline α-Fe, Acta Mater 264 (2024) 119541, https://doi.org/10.1016/j.actamat.2023.119541.
[15] G.B. Bizana, L.A. Barrales-Mora, Kinetics of grain boundary migration in nanosized Al polycrystals, Acta Mater 206 (2023) 119261, https://doi.org/10.1016/j.actamat.2023.119261.
[16] M. Lyu, Z. Xu, G.S. Rohrer, E.A. Holm, Comparing molecular dynamics simulations of grain growth with experimental data, Scripta Mater 256 (2025) 116429, https://doi.org/10.1016/j.scriptamat.2024.116429.
[17] S.K. Naghibzadeh, Z. Xu, D. Kinderlehrer, R. Suter, K. Dayal, G.S. Rohrer, Impact of grain boundary energy anisotropy on grain growth, Phys. Rev. Mater. 8 (2024) 093403, https://doi.org/10.1103/PhysRevMaterials.8.093403.
[18] J. Zhang, W. Ludwig, Y.B. Zhang, H.H.B. Sorensen, D.J. Rowenhorst, A. Yamanaka, P.W. Voorhees, H.F. Poulsen, Grain boundary mobilities in polycrystals, Acta Mater 191 (2020) 211–220, https://doi.org/10.1016/j.actamat.2020.03.044.
[19] G. Gottstein, D.A. Molodov, L.S. Shvindlerman, Grain boundary migration in metals: Recent developments, Interface Sci 6 (1998) 7–22, https://doi.org/10.1023/a:1008641617937.
[20] J.M. Dake, J. Oddershede, H.O. Sorensen, T. Werz, J.C. Shatto, K. Uesugi, S. Schmidt, C.E. Krill, III, Direct observation of grain rotations during coarsening of a semisolid Al-Cu alloy, Proc. Natl. Acad. Sci. U.S.A. 113 (2016) E5998–E6006, https://doi.org/10.1073/pnas.1602293113.
[21] J. Sun, J.M. Dake, J. Oddershede, Grain structure evolution during heat treatment of a semisolid Al-Cu alloy studied with lab-based diffraction contrast tomography, Tomography of Materials and Structures 4 (2024) 100025, https://doi.org/10.1016/j.tmater.2024.100025.
[22] Z. Xu, C.M. Hefferan, S.F. Li, J. Lind, R.M. Suter, F. Abdeljawad, G.S. Rohrer, Energy dissipation by grain boundary replacement during grain growth, Scripta Mater 230 (2023) 115405, https://doi.org/10.1016/j.scriptamat.2023.115405.
[23] T. Massalski, Binary Alloy Phase Diagram, 3rd Ed., ASM International, Materials Park, OH, 1996.
[24] J. Sun, J. Oddershede, J. Dake. Grain structure evolution during heat treatment of a Al-5wt%Cu alloy studied with lab-based diffraction contrast tomography. The Materials Data Facility: http://doi.org/10.18126/5q8s-3ef9, 2023.
[25] D.M. Saylor, B.S. El Dasher, A.D. Rollett, G.S. Rohrer, Distribution of grain boundaries in aluminum as a function of five macroscopic parameters, Acta Mater 52 (2004) 3649–3655, https://doi.org/10.1016/j.actamat.2004.04.018.
[26] F. Bachmann, H. Bale, N. Gueninchault, C. Holzner, E.M. Lauridsen, 3D grain reconstruction from laboratory diffraction contrast tomography, J. Appl. Crystallogr. 52 (2019) 643–651, https://doi.org/10.1107/S1600576719005442.
[27] M.A. Groeber, M.A. Jackson, DREAM.3D: A Digital Representation Environment for the Analysis of Microstructure in 3D, Integr. Mater. Manuf. I. 3 (2014) 56–72, https://doi.org/10.1186/2193-9772-3-5.
[28] J. Goldfeather, V. Interrante, A novel cubic-order algorithm for approximating principal direction vectors, ACM Trans. Graph. 23 (2004) 45–63, https://doi.org/10.1145/966131.966134.
[29] X.T. Zhong, D.J. Rowenhorst, H. Beladi, G.S. Rohrer, The five-parameter grain boundary curvature distribution in an austenitic and ferritic steel, Acta Mater 123 (2017) 136–145, https://doi.org/10.1016/j.actamat.2016.10.030.
[30] D.J. Rowenhorst, J.P. Kuang, K. Thornton, P.W. Voorhees, Three-dimensional analysis of particle coarsening in high volume fraction solid-liquid mixtures, Acta Mater 54 (2006) 2027–2039, https://doi.org/10.1016/j.actamat.2005.12.038.
[31] D.J. Rowenhorst, P.W. Voorhees, Measurements of the grain boundary energy and anisotropy in tin, Metallurgical and Materials Transactions A-Physical Metallurgy and Materials Science 36A (2005) 2127–2135, https://doi.org/10.1007/s11661-005-0333-7.
[32] Y.F. Shen, X.T. Zhong, H. Liu, R.M. Suter, A. Morawiec, G.S. Rohrer, Determining grain boundary energies from triple junction geometries without discretizing the five-parameter space, Acta Mater 166 (2019) 126–134, https://doi.org/10.1016/j.actamat.2018.12.022.
[33] C. Herring, Structure and Properties of Solid Surfaces; proceedings of a conference arranged by the National Research Council and held in September, 1952, in: R. Gomer, C.S. Smith (Eds.), The Use of Classical Macroscopic Concepts in Surface Energy Problems, University of Chicago Press, Chicago, 1953, pp. 5–81, in Lake Geneva, Wisconsin, USA.
[34] A.V. Knyazev, Toward the optimal preconditioned eigensolver: Locally optimal block preconditioned conjugate gradient method, SIAM J. Sci. Comput. 23 (2001) 517–541, https://doi.org/10.1137/S1064827500366124.

[35] K. Glowinski, A. Morawiec, Analysis of Experimental Grain Boundary Distributions Based on Boundary-Space Metrics, Metall. Mater. Trans. A 45A (2014) 3189–3194, https://doi.org/10.1007/s11661-014-2325-y.
[36] G.S. Rohrer, 3D_dist_graph. https://github.com/gr20cmu/gbXstallography/tree/main/3D_dist_graph, 2023.
[37] B. Merriman, J.K. Bence, S.J. Osher, Motion of multiple junctions - a level set approach, J. Comp. Phys. 112 (1994) 334–363, https://doi.org/10.1006/jcph.1994.1105.
[38] B.B. Merriman, J.K. Osher, Diffusion Generated Motion by Mean Curvature, Department of Mathematics, *S.*, University of California, Los Angeles, 1992.
[39] X. Peng, A. Bhattacharya, S.K. Naghibzadeh, D. Kinderlehrer, R. Suter, K.K. Dayal, G.S. Rohrer, Comparison of simulated and measured grain volume changes during grain growth, Phys. Rev. Mater. 6 (2022) 033402, https://doi.org/10.1103/PhysRevMaterials.6.033402.
[40] J.X. Peng, Grain Growth TD iso (2021). https://github.com/JadeXiaoyaoPeng/GrainGrowth_TD_iso.
[41] J.M. Dake. Experimental Investigations of Microstructural Coarsening in 3D using X-Ray Microscopy. der Fakultät für Ingenieurwissenschaften, Informatik und Psychologie, vol. Ph.D. Ulm: Universität Ulm, 2019.
[42] S.C. Hardy, P.W. Voorhees, Ostwald ripening in a system with a high volume fraction of coarsening phase, Metall. Trans. A 19 (1988) 2713–2721, https://doi.org/10.1007/BF02645806.
[43] R. Mendoza, J. Alkemper, P.W. Voorhees, Three-dimensional morphological characterization of coarsened microstructures, Z Metallkd 96 (2005) 155–160, https://doi.org/10.3139/146.101013.
[44] D.J. Rowenhorst, A.C. Lewis, G. Spanos, Three-dimensional analysis of grain topology and interface curvature in a beta-titanium alloy, Acta Mater 58 (2010) 5511–5519, https://doi.org/10.1016/j.actamat.2010.06.030.
[45] J. Gruber, H.M. Miller, T.D. Hoffmann, G.S. Rohrer, A.D. Rollett, Misorientation texture development during grain growth. Part I: Simulation and experiment, Acta Mater 57 (2009) 6102–6112, https://doi.org/10.1016/j.actamat.2009.08.036.
[46] J. Niño, O.K. Johnson, Evolution of crystallographic texture and grain boundary network structure during anisotropic grain growth, Comput. Mater. Sci. 240 (2024) 113023, https://doi.org/10.1016/j.commatsci.2024.113023.
[47] D.J. Rowenhorst, P.W. Voorhees, Measurement of Interfacial Evolution in Three Dimensions, Ann. Rev. Mater. Res. 42 (2012) 105–124, https://doi.org/10.1146/annurev-matsci-070511-155028.
[48] G.S. Rohrer, Grain boundary energy anisotropy: a review, J. Mater. Sci. 46 (2011) 5881–5895, https://doi.org/10.1007/s10853-011-5677-3.
[49] N. Lu, S. Moniri, M.R. Wiltse, J. Spielman, N. Senabulya, A.J. Shahani, Dynamics of Ga penetration in textured Al polycrystal revealed through multimodal three-dimensional analysis, Acta Mater 217 (2021) 117145, https://doi.org/10.1016/j.actamat.2021.117145.
[50] J. Sun, Y. Zhang, A. Lyckegaard, F. Bachmann, E.M. Lauridsen, D.J. Jensen, Grain boundary wetting correlated to the grain boundary properties: A laboratory-based multimodal X-ray tomography investigation, Scripta Mater 163 (2019) 77–81, https://doi.org/10.1016/j.scriptamat.2019.01.007.
[51] S.J. Dillon, G.S. Rohrer, Mechanism for the development of anisotropic grain boundary character distributions during normal grain growth, Acta Mater 57 (2009) 1–7, https://doi.org/10.1016/j.actamat.2008.08.062.

Supplemental information for:
Grain boundary properties and microstructure evolution in an Al-Cu alloy

Zipeng Xu[1], Jun Sun[2], Jules M. Dake[3], Jette Oddershede[2], Harpreet Kaur[4], S. Kiana Naghibzadeh[4], Carl E. Krill III[3], Kaushik Dayal[4], and Gregory S. Rohrer[1]

[1]Department of Materials Science and Engineering, Carnegie Mellon University

[2]Xnovo Technology ApS, Galoche Allé 15, 1st floor, 4600 Køge, Denmark

[3]Institute of Functional Nanosystems, Ulm University, 89081 Ulm, Germany

[4]Department of Civil and Environmental Engineering, Carnegie Mellon University

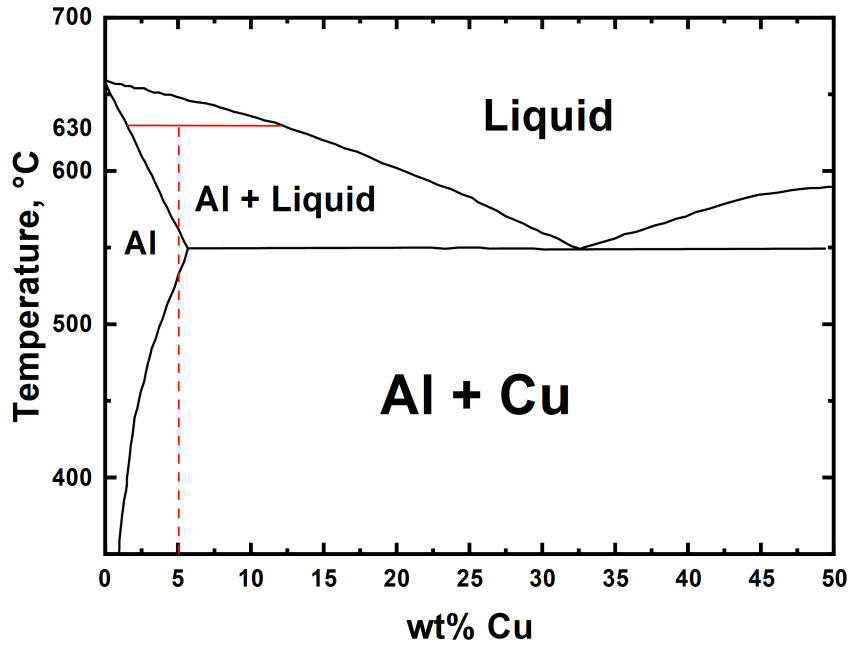

Figure S1. The Al-Cu binary phase diagram. The red solid line represents the temperature of heat treatment (630°C), and the red dashed line represents the equilibrium cooling path of the experimental sample (Al-5 wt% Cu).

The phase diagram in Fig. S1 can be used to determine the microstructure expected with the Al-Cu alloy solidifies from the melting point. Along the equilibrium cooling path, the boundaries that form on solidification are between the Al-rich solid solution phase with 5 wt%

Cu. In other words, they are homophase grain boundaries. At a lower temperature (≈ 530 °C), small amounts of Al_2Cu precipitate out. These precipitates are too small to be detected by DCT. If the semi-solid were instead quenched instantaneously from the annealing temperature, the equilibrium intergranular liquid would be about 12 wt% Cu. If this solidified at the eutectic temperature, it would yield a mixture of the Al solid solution phase and Al_2Cu precipitates with a microstructure finer than the DCT resolution. In reality, the microstructure is somewhere between these limits. What we can surmise is that, regardless of the details, the aluminum solid solution will be a continuous phase, and fine-scale Al_2Cu will be precipitated in the areas that were liquid at the annealing temperature. The liquid fraction at the process temperature is estimated to be 30 % after accounting for the fraction trapped within grains and does not influence the interfaces, as in reference [1].

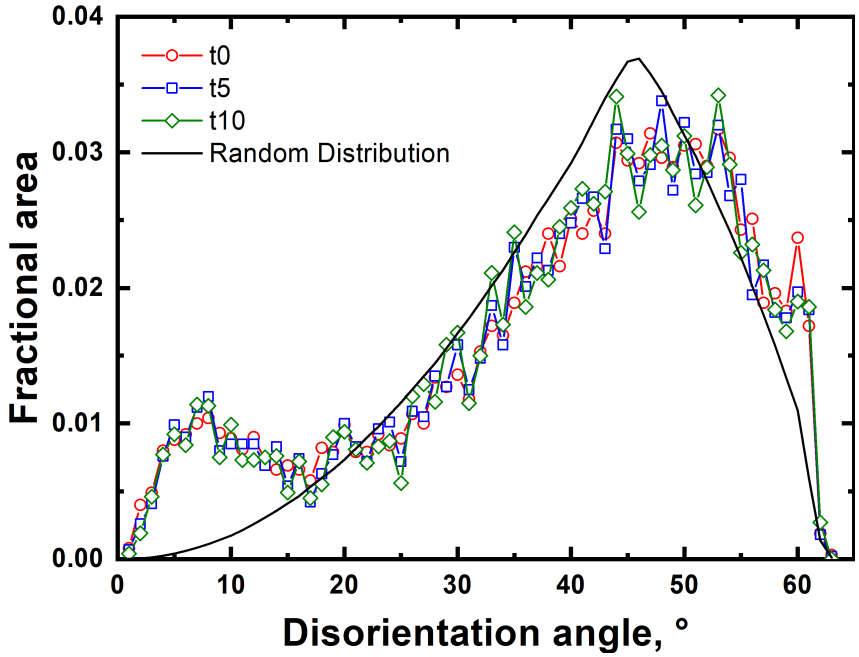

Figure S2. The disorientation distribution of a random distribution of grain orientations, and the disorientation distributions of the Al-5 wt% Cu sample at times $t_0 = 0$, $t_5 = 75$, and $t_{10} = 150$ mins.

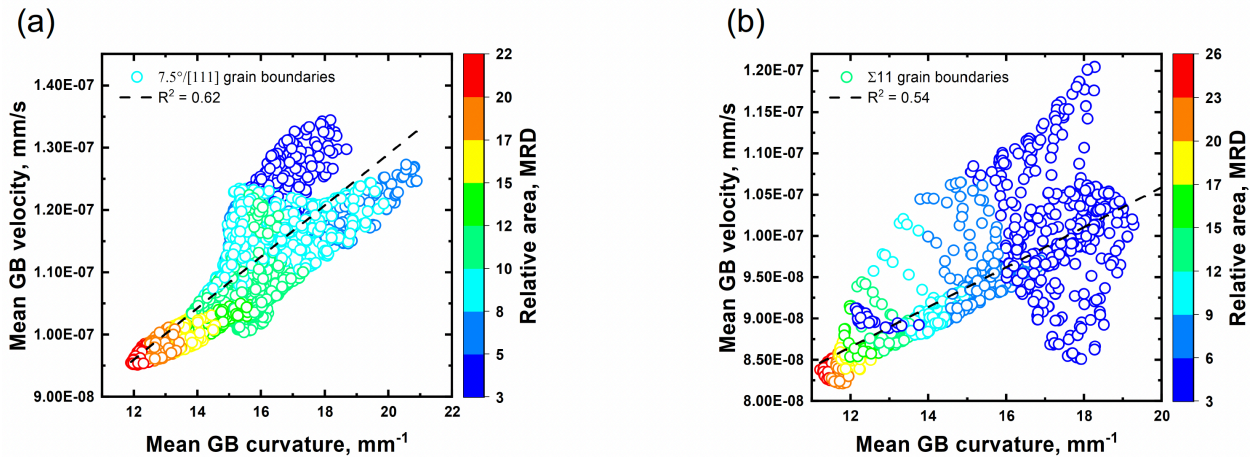

Figure S3. The velocity and curvature of various types of grain boundary with corresponding linear fitting. Each data point represents one grain boundary plane's normal orientation and is colored by the corresponding relative area in units of MRD. (a) 7.5°/[111] low-angle grain boundaries; (b) 50.5°/[110] Σ11 grain boundaries. There are 833 observations of 7.5°/[111] low-angle grain boundaries and 548 observations of Σ11 grain boundaries.

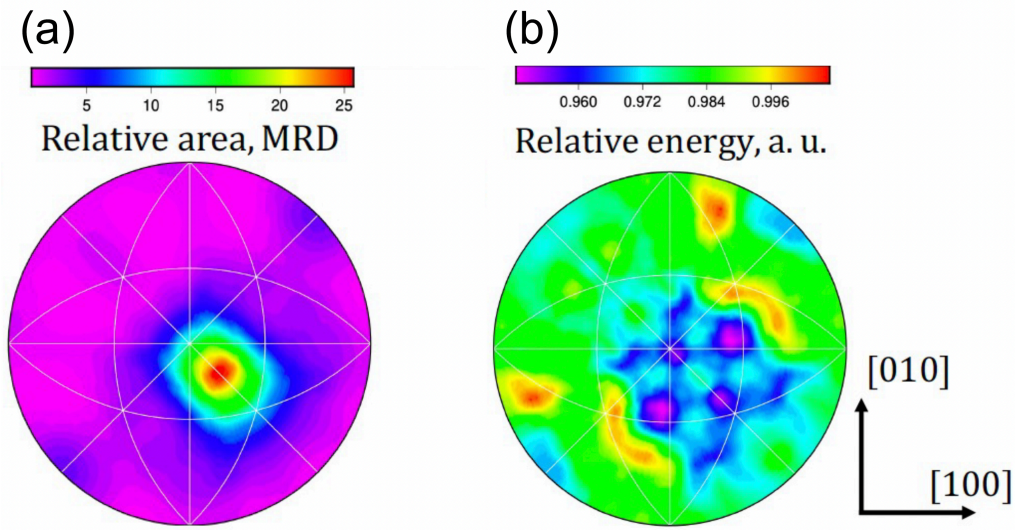

Figure S4. The grain boundary (a) relative area and (b) relative energy distributions for 50.5°/[110] Σ11 grain boundaries.

References Cited

[1] T. Werz, M. Baumann, U. Wolfram, C.E. Krill. Particle tracking during Ostwald ripening using time-resolved laboratory X-ray microtomography, Mater. Charact. 90 (2014) 185-195, http://dx.doi.org/10.1016/j.matchar.2014.01.022.